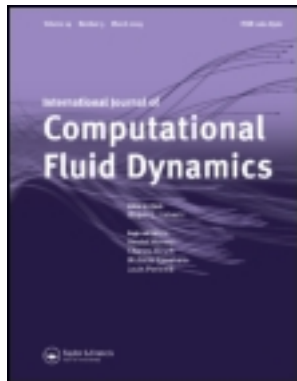


This article was downloaded by: [Christo Christov]

On: 13 October 2011, At: 20:15

Publisher: Taylor & Francis

Informa Ltd Registered in England and Wales Registered Number: 1072954 Registered office: Mortimer House, 37-41 Mortimer Street, London W1T 3JH, UK



## International Journal of Computational Fluid Dynamics

Publication details, including instructions for authors and subscription information:

<http://www.tandfonline.com/loi/gcfd20>

### A Fully Coupled Solver for Incompressible Navier-Stokes Equations using Operator Splitting

R.S. Marinova\*<sup>a</sup>, C.I. Christov<sup>b</sup> & T.T. Marinov†<sup>c</sup>

<sup>a</sup> Computational Science Division, National Aerospace Laboratory, Jindaiji-Higashi-machi-1 Chofu, 182-8522, Tokyo, Japan;

<sup>b</sup> Department of Mathematics, University of Louisiana at Lafayette, 70504-1010, Lafayette, LA, USA

<sup>c</sup> Department of Mathematical Sciences, University of Alberta, T6G 2G1, Edmonton, Alberta, Canada

Available online: 10 Oct 2011

To cite this article: R.S. Marinova\*, C.I. Christov & T.T. Marinov† (2011): A Fully Coupled Solver for Incompressible Navier-Stokes Equations using Operator Splitting, International Journal of Computational Fluid Dynamics, 17:5, 371-385

To link to this article: <http://dx.doi.org/10.1080/1061856031000114300>

PLEASE SCROLL DOWN FOR ARTICLE

Full terms and conditions of use: <http://www.tandfonline.com/page/terms-and-conditions>

This article may be used for research, teaching, and private study purposes. Any substantial or systematic reproduction, redistribution, reselling, loan, sub-licensing, systematic supply, or distribution in any form to anyone is expressly forbidden.

The publisher does not give any warranty express or implied or make any representation that the contents will be complete or accurate or up to date. The accuracy of any instructions, formulae, and drug doses should be independently verified with primary sources. The publisher shall not be liable for any loss, actions, claims, proceedings, demand, or costs or damages whatsoever or howsoever caused arising directly or indirectly in connection with or arising out of the use of this material.

# A Fully Coupled Solver for Incompressible Navier–Stokes Equations using Operator Splitting

R.S. MARINOVA<sup>a,\*</sup>, C.I. CHRISTOV<sup>b,†</sup> and T.T. MARINOV<sup>c,‡</sup>

<sup>a</sup>Computational Science Division, National Aerospace Laboratory, Jindaiji-Higashi-machi 7-44-1 Chofu, Tokyo 182-8522, Japan;

<sup>b</sup>Department of Mathematics, University of Louisiana at Lafayette, Lafayette, LA 70504-1010, USA; <sup>c</sup>Department of Mathematical Sciences, University of Alberta, Edmonton, Alberta, Canada, T6G 2G1

(Received 16 January 2002; In final form 3 January 2003)

The steady incompressible Navier–Stokes equations are coupled by a Poisson equation for the pressure from which the continuity equation is subtracted. The equivalence to the original N–S problem is proved. Fictitious time is added and vectorial operator-splitting is employed leaving the system coupled at each fractional-time step which allows satisfaction of the boundary conditions without introducing artificial conditions for the pressure. Conservative second-order approximations for the convective terms are employed on a staggered grid. The splitting algorithm for the 3D case is verified through an analytic solution test. The stability of the method at high values of Reynolds number is illustrated by accurate numerical solutions for the flow in a lid-driven rectangular cavity with aspect ratio 1 and 2, as well as for the flow after a back-facing step.

**Keywords:** Incompressible flows; Operator-splitting; High Reynolds numbers; Navier–Stokes equations

## INTRODUCTION

A fully implicit coupled method for solving Navier–Stokes equations has been proposed in Christov and Marinova (1998a) for the two-dimensional case, where a modified equation for pressure is used instead of the continuity equation. The formulation with pressure equation requires the continuity equation to be satisfied at the boundary. This method can be viewed as an extension to the case of primitive variables of the method of false transients—a time derivative with respect to artificial time is added in the modified pressure Poisson equation. In order to minimize the computational cost, the resulting system is solved by coordinate operator-splitting which is preferable in our work (comparing with pressure–velocity decoupling) not only for computational efficiency but also for stability reasons. In Christov and Marinova (1998a,b; 2001) a special treatment for the split operators is proposed which leaves the pressure function coupled to one of the velocity components. Thus no artificial boundary conditions are needed for the pressure and the scheme can be fully implicit. To enhance the stability, fully coupled methods with various

forms of continuity or pressure equations are often used in the literature, see Mallison and de Vahl Davis (1973), Soh (1987), Habashi *et al.* (1993) and Hafez and Soliman (1993).

In this work, our main goal is to present the new method and to illustrate its effectiveness for obtaining the steady-state numerical solution at high Reynolds numbers using fine grids. The article is organized in sections as follows: the problem is introduced in the second section, where the modified equation for pressure is derived and the method of false transients is applied. Next, in the third section, the vectorial operator splitting method for solving the obtained evolution problem is presented, while the difference approximation and respective algorithm for solving the difference problem are described in the fourth and fifth sections. To demonstrate the properties and abilities of the method, in the sixth section we present and discuss some numerical results for different problems: test with 3D analytic solution and 2D lid-driven flow in a cavity. Accurate numerical solutions for the flow over a backward-facing step in a channel are obtained for high Reynolds numbers extending the parameter range of our previous computations (Marinova *et al.* (2000)).

\*E-mail: marinova@nal.go.jp

†Corresponding author. E-mail: christov@louisiana.edu

‡E-mail: marinov@ualberta.ca

The seventh section summarizes the results obtained in the present paper.

## PROBLEM FORMULATION

Consider the steady incompressible Navier–Stokes equations

$$\frac{1}{Re} \Delta \mathbf{u} - \nabla p - C[\mathbf{u}] = \mathbf{f} \quad (1)$$

coupled by the continuity equation

$$\nabla \cdot \mathbf{u} = 0 \quad (2)$$

in a bounded compact domain  $\Omega$  with a piece wise smooth boundary  $\partial\Omega$ . Here  $x \in \Omega$ ,  $\mathbf{u} = \mathbf{u}(\mathbf{x})$  is the velocity vector,  $p = p(\mathbf{x})$  is the pressure and  $\mathbf{f} = \mathbf{f}(\mathbf{x})$  is the force vector. The Reynolds number is defined as  $Re = UL/\nu$ , where  $U$  is the characteristic velocity,  $L$  is the characteristic length and  $\nu$  is the kinematic coefficient of viscosity.

In numerical solution of the incompressible Navier–Stokes equations the determination of the pressure field is a serious task. If a portion of  $\partial\Omega$  is a free boundary then the non-flux conditions for the velocity, say  $\mathbf{u} \cdot \mathbf{n} = v_n$ , together with the magnitude of the pressure are specified. Such a case is simpler since one gets an explicit condition for each function at the boundary. The case of internal flows with no free boundaries is more complicated because the pressure  $p$  is an implicit function and no boundary conditions are available for it. In our consideration we assume that the velocity is prescribed at the boundary  $\partial\Omega$

$$\mathbf{u}|_{\partial\Omega} = \mathbf{u}_b. \quad (3)$$

In Eq. (1) the operator  $C[\mathbf{u}]$  is a short-hand notation for the advection term. For this term we use the skew-symmetric form

$$\begin{aligned} C[\mathbf{u}] &= \frac{1}{2} [\nabla \cdot (\mathbf{u}\mathbf{u}) + \mathbf{u} \cdot \nabla \mathbf{u}] = (\mathbf{u} \cdot \nabla) \mathbf{u} + \frac{1}{2} \mathbf{u} (\nabla \cdot \mathbf{u}) \\ &= \nabla \cdot (\mathbf{u}\mathbf{u}) - \frac{1}{2} \mathbf{u} (\nabla \cdot \mathbf{u}), \end{aligned} \quad (4)$$

which follows from the continuity Eq. (2). It is readily shown that the operator  $C$  is skew-symmetric for any  $\mathbf{u}$  from the considered space with trivial boundary conditions, namely

$$\begin{aligned} (C[\mathbf{u}], \mathbf{u}) &= \int_{\Omega} \mathbf{u} \cdot C[\mathbf{u}] \, dx = \int_{\Omega} \frac{1}{2} \mathbf{u} \cdot [\nabla \cdot (\mathbf{u}\mathbf{u}) + \mathbf{u} \cdot \nabla \mathbf{u}] \, dx \\ &= \int_{\Omega} \frac{1}{2} [\mathbf{u} \cdot \nabla (\mathbf{u}^2) + \mathbf{u}^2 \cdot \nabla \mathbf{u}] \, dx \\ &= \int_{\Omega} \frac{1}{2} [\nabla \cdot (\mathbf{u}\mathbf{u}^2)] \, dx = \oint_{\partial\Omega} \frac{1}{2} \mathbf{u}^2 v_n \, ds = 0. \end{aligned} \quad (5)$$

Moreover, for the nonlinear operators in each direction

$$\begin{aligned} C_x[\varphi] &= \frac{1}{2} \left[ \frac{\partial(\varphi u)}{\partial x} + u \frac{\partial \varphi}{\partial x} \right], \quad C_y[\varphi] = \frac{1}{2} \left[ \frac{\partial(\varphi v)}{\partial y} + v \frac{\partial \varphi}{\partial y} \right], \\ C_z[\varphi] &= \frac{1}{2} \left[ \frac{\partial(\varphi w)}{\partial x} + w \frac{\partial \varphi}{\partial z} \right], \end{aligned}$$

under the assumption of homogenous boundary conditions we have

$$(C_x[\varphi], \varphi) = (C_y[\varphi], \varphi) = (C_z[\varphi], \varphi) = 0. \quad (6)$$

Here  $\varphi$  is one of the velocity components  $u$ ,  $v$  and  $w$ . For instance, in direction  $x$

$$(C_x[\varphi], \varphi) = \int_{\Omega} \frac{\varphi}{2} \left[ \frac{\partial(\varphi u)}{\partial x} + u \frac{\partial \varphi}{\partial x} \right] \, dx = \frac{1}{2} \int_{\Omega} \frac{\partial(\varphi^2 u)}{\partial x} \, dx = 0. \quad (7)$$

## Pressure Equation

Instead of the continuity equation we use a Poisson equation for pressure. This equation is derived from the well-known ‘‘Poisson equation for pressure’’

$$\Delta p + \nabla \cdot (C[\mathbf{u}] + \mathbf{f}) = 0 \quad (8)$$

after multiplying Eq. (8) by  $1/Re$  and from the result subtracting the continuity Eq. (2). In this way one obtains an explicit relation for the pressure  $p$

$$\frac{1}{Re} \Delta p - \nabla \cdot \mathbf{u} + \frac{1}{Re} \nabla \cdot (C[\mathbf{u}] + \mathbf{f}) = 0. \quad (9)$$

The formulation with the equation for pressure (9) is equivalent to the original system only if the continuity Eq. (2) is also satisfied on the boundary, namely

$$\Delta \cdot \mathbf{u}|_{\partial\Omega} = 0. \quad (10)$$

Thus we arrive at a new boundary-value problem (1), (9) with boundary conditions (3), (10) for the primitive variables  $\mathbf{u}$  and  $p$  which is equivalent to the original problem. Any solution of the system (1), (9), subject to the boundary conditions (3), (10), is a solution of the original boundary value problem (1)–(3). The proof of this statement can be obtained in the following way: apply the operator  $\nabla$  to Eq. (1) and from the result subtract Eq. (9) multiplied by  $Re$ . Then for the divergence  $\nabla \cdot \mathbf{u}$  we get the following boundary-value problem

$$\begin{aligned} \Delta(\nabla \cdot \mathbf{u}) - Re^2(\nabla \cdot \mathbf{u}) &= 0 \quad \text{for } \mathbf{x} \in \Omega; \\ \nabla \cdot \mathbf{u} &= 0 \quad \text{for } \mathbf{x} \in \partial\Omega, \end{aligned} \quad (11)$$

with Eq. (10) duly acknowledged. The boundary value problem (11) has a unique trivial solution, hence the continuity Eq. (2) is satisfied in the entire domain  $\Omega$ .

The above statement provides the sufficient condition for one-to-one correspondence between the two formulations. The necessity follows directly from the way the new system is derived. Hence the equivalence between the two boundary value problems is established.

### Evolution System

To compute the stationary solution we render the system to an evolution system by adding in each equation of the governing system (1), (9), derivatives with respect to an *artificial* time  $t$ . Thus, we obtain the following parabolic problem

$$\frac{\partial \mathbf{u}}{\partial t} = \frac{1}{Re} \Delta \mathbf{u} - \nabla p - C[\mathbf{u}] - \mathbf{f}, \quad (12)$$

$$\frac{\partial p}{\partial t} = \frac{1}{Re} \Delta p - \nabla \cdot \mathbf{u} + \frac{1}{Re} (\nabla \cdot C[\mathbf{u}] + \mathbf{f}). \quad (13)$$

This is not the real physical non-stationary problem. The system (12), (13) has no physical meaning until a steady state is reached. A similar procedure has been proposed by Mallison and de Vahl Davis (1973) for the  $\psi - \omega$  formulation and called "Method of False Transients". The parabolic system (12) and (13) can be viewed as an extension to the case of primitive variables. The pseudo-time step is an additional parameter in the scheme that can be varied to accelerate convergence. Upon convergence, the pseudo-time term vanishes, and Eqs. (1) and (9) are satisfied. Here, it is to be mentioned that dynamical properties of the system (12), (13) can have little in common with the dynamics of the real time-dependent problem. What matters in the Method of False Transients is the stationary solution obtained after the time-stepping converges. A different kind of false-transient algorithm (artificial compressibility) was used in Soh (1987) where a time derivative of pressure was added to the continuity equation.

One should note that the main difference between *the false transients* and *artificial compressibility* is that the former leads to a system which is parabolic while the latter results in a system which is hyperbolic in the space of solenoidal functions (vector functions of zero divergence).

We render the system for  $\mathbf{u}$  and  $p$  into the following vectorial system

$$\frac{\partial \boldsymbol{\theta}}{\partial t} = L[\boldsymbol{\theta}] + N[\boldsymbol{\theta}] + F[\boldsymbol{\theta}], \quad (14)$$

where

$$\boldsymbol{\theta} = \begin{pmatrix} \mathbf{u} \\ p \end{pmatrix}, \quad L = \begin{pmatrix} \Delta/Re & -\nabla \\ -\nabla & \Delta/Re \end{pmatrix}, \quad N = \begin{pmatrix} -C & 0 \\ 0 & 0 \end{pmatrix},$$

$$F[\boldsymbol{\theta}] = \begin{pmatrix} -\mathbf{f} \\ \nabla \cdot (C[\mathbf{u}] + \mathbf{f})/Re \end{pmatrix}.$$

The boundary conditions are Eqs. (3) and (10).

In incompressible flows the pressure is defined up to an arbitrary function of time. For the sake of convenience we define this function similarly to Abdallah (1987) as the average of the pressure at the specific time stage, i.e. we assume (for pressure uniqueness) that the following relation is satisfied

$$\int_{\Omega} p(\mathbf{x}, t) \, d\mathbf{x} = 0, \quad t > 0. \quad (15)$$

### OPERATOR SPLITTING

We employ a generalization of the scheme of Douglas and Rachford (1956). One of the main reasons for our choice to make use of this particular scheme is that it can be applied in the three-dimensional case as well. For splitting the operator  $A = A_1 + \dots + A_l$  in the equation

$$\frac{\partial \boldsymbol{\theta}}{\partial t} = A\boldsymbol{\theta} + G \quad (16)$$

we make the following steps

$$\frac{\boldsymbol{\theta}^{m+1/l} - \boldsymbol{\theta}^m}{\tau} = A_1 \boldsymbol{\theta}^{m+1/l} + \sum_{i=2}^l A_i \boldsymbol{\theta}^m + G^m \quad (17)$$

$$\frac{\boldsymbol{\theta}^{m+i/l} - \boldsymbol{\theta}^{m+(i-1)/l}}{\tau} = A_i (\boldsymbol{\theta}^{m+i/l} - \boldsymbol{\theta}^m), \quad (18)$$

$$i = 2, \dots, l,$$

where  $l=2$  and  $l=3$  in two- and three-dimensional cases, respectively. The splitting scheme approximates the fully implicit backward scheme. We are interested in the converged solution and therefore the order of approximation with respect to the artificial time is not important. Note that the first fractional step produces consistency with the equation, and the next steps are introduced to improve the stability. For this reason the splitting scheme is called a scheme with stabilizing correction, see Yanenko (1971).

After excluding  $\boldsymbol{\theta}^{m+i/l}$ ,  $i = 1, \dots, l-1$ , from Eqs. (17) and (18) the scheme in whole step adopts the form

$$\prod_{i=1}^l (I - \tau A_i) \frac{\boldsymbol{\theta}^{m+1} - \boldsymbol{\theta}^m}{\tau} = A\boldsymbol{\theta}^m + G^m. \quad (19)$$

We take

$$A_1 = L_x + N_x, \quad A_2 = L_y + N_y, \quad A_3 = L_z + N_z, \quad (20)$$

where  $L_x, N_x$  are the respective operators of the derivatives with respect to  $x$ ,  $L_y, N_y$  - with respect to  $y$ , and  $L_z, N_z$  - with respect to  $z$ -direction.

The above splitting scheme (19) has the desirable property that, if the numerical solution converges, its steady state solutions are *independent* of the time

increment. It is readily seen that upon convergence,  $\|\boldsymbol{\theta}^{m+1} - \boldsymbol{\theta}^m\| \rightarrow 0$ , the expression for the error in approximation of the steady-state equations does not involve the increment of the artificial time.

The main advantage is that due to the economy of the computer time and memory required, the schemes of stabilizing correction are very efficient for solving multidimensional problems. The operator-splitting schemes are economical as explicit schemes and can retain the unconditional stability inherent in some of the implicit schemes.

## DIFFERENCE SCHEME

We choose the approximations of the differential equations and boundary conditions for which the numerical scheme preserves the integral properties of the respective differential problem. For finite difference schemes it is not a trivial task especially in the case of operator-splitting.

For the case under consideration, the flow occupies the region with rectilinear boundaries in Cartesian coordinates. The boundary conditions deriving from the continuity Eq. (10) in the three-dimensional case read

$$\begin{aligned} \left. \frac{\partial u}{\partial x} \right|_{(x=c,y,z)} &= g_1(y,z), & \left. \frac{\partial v}{\partial y} \right|_{(x,y=c,z)} &= g_2(x,z), \\ \left. \frac{\partial w}{\partial z} \right|_{(x,y,z=c)} &= g_3(x,y), \end{aligned} \quad (21)$$

where  $(x = c, y, z)$ ,  $(x, y = c, z)$ , and  $(x, y, z = c)$  are boundary points;  $c$  is a generic constant, which can be different;  $g_i$ ,  $i = 1, 2, 3$  are known functions obtained from Eqs. (3) and (10). We keep the coupling between the pressure and the respective velocity component through the boundary conditions at each fractional time step. It allows us to construct an efficient implicit splitting scheme.

The grid is *staggered* for  $u$  in  $x$ -direction, for  $v$  in  $y$ -direction, and for  $w$  in  $z$ -direction. For boundary conditions involving derivatives this allows one to use central differences with second order of approximation on two-point stencils. The number of main grid lines (which are, in fact, the  $p$ -grid lines) in the  $x$ -,  $y$ - and  $z$ -directions are, respectively,  $N_x$ ,  $N_y$  and  $N_z$ . The coordinates of the grid points are  $(x_i, y_j, z_k)$  for  $i = 1, \dots, N_x$ ,  $j = 1, \dots, N_y$ ,  $k = 1, \dots, N_z$ . The spacings are given by  $h_{x,i}^p = x_{i+1} - x_i$ ,  $i = 1, \dots, N_x - 1$ ,  $h_{y,j}^p = y_{j+1} - y_j$ ,  $j = 1, \dots, N_y - 1$ , and  $h_{z,k}^p = z_{k+1} - z_k$ ,  $k = 1, \dots, N_z - 1$ . The spacings for the function  $u$  in direction  $x$  are defined as follows

$$\begin{aligned} h_{x,1}^u &= h_{x,1}^p, & h_{x,i}^u &= \frac{1}{2} (h_{x,i}^p + h_{x,i-1}^p) \\ \text{for } i &= 2, \dots, N_x - 1, & \text{and } h_{x,N_x}^u &= h_{x,N_x-1}^p. \end{aligned}$$

Similarly the spacings for  $v$  in direction  $y$  and for  $w$  in direction  $z$  are defined

$$\begin{aligned} h_{y,1}^v &= h_{y,1}^p, & h_{y,j}^v &= \frac{1}{2} (h_{y,j}^p + h_{y,j-1}^p) \\ \text{for } j &= 2, \dots, N_y - 1, & \text{and } h_{y,N_y}^v &= h_{y,N_y-1}^p, \end{aligned} \quad (22)$$

$$\begin{aligned} h_{z,1}^w &= h_{z,1}^p, & h_{z,k}^w &= \frac{1}{2} (h_{z,k}^p + h_{z,k-1}^p) \\ \text{for } k &= 2, \dots, N_z - 1, & \text{and } h_{z,N_z}^w &= h_{z,N_z-1}^p. \end{aligned} \quad (23)$$

The pressure is sampled at the points labelled by “•”; function  $u$  - at “◦”; function  $v$  - at “\*”, and function  $w$  - at “◊”. The following notations are used

$$\begin{aligned} p_{i,j,k} &= p(x_i, y_j, z_k), \\ u_{i,j,k} &= u\left(x_i - \frac{1}{2}h_{x,i-1}^p, y_j, z_k\right), \\ v_{i,j,k} &= v\left(x_i, y_j - \frac{1}{2}h_{y,j-1}^p, z_k\right), \\ w_{i,j,k} &= w\left(x_i, y_j, z_k - \frac{1}{2}h_{z,k-1}^p\right). \end{aligned} \quad (24)$$

For the second derivatives, standard three point difference approximations are employed, which inherit the negative definiteness of the respective differential operators. For instance, in direction  $x$  the approximation has the form

$$\begin{aligned} \left. \frac{\partial^2 f}{\partial x^2} \right|_{i,j,k} &\approx \frac{2}{h_{x,i}^f + h_{x,i-1}^f} \\ &\times \left( \frac{f_{i+1,j,k} - f_{i,j,k}}{h_{x,i}^f} - \frac{f_{i,j,k} - f_{i-1,j,k}}{h_{x,i-1}^f} \right), \end{aligned} \quad (26)$$

where  $f$  stands for one of the functions  $u$ ,  $v$ ,  $w$  or  $p$ .

The first derivatives for pressure at the mesh-point labelled by “◦”, “\*”, and “◊” are approximated in the following way:

$$\begin{aligned} \left. \frac{\partial p}{\partial x} \right|_{\circ} &\approx \frac{p_{i,j,k} - p_{i-1,j,k}}{h_{x,i-1}^p}, & \left. \frac{\partial p}{\partial y} \right|_{*} &\approx \frac{p_{i,j,k} - p_{i,j-1,k}}{h_{y,j-1}^p}, \\ \left. \frac{\partial p}{\partial z} \right|_{\diamond} &\approx \frac{p_{i,j,k} - p_{i,j,k-1}}{h_{z,k-1}^p}. \end{aligned} \quad (27)$$

On the other hand, the derivatives  $\partial u/\partial x$ ,  $\partial v/\partial y$ , and  $\partial w/\partial z$  in  $\nabla \cdot \mathbf{u}$  at each interior mesh-point labelled by “•”

are approximated as

$$\begin{aligned} \frac{\partial u}{\partial x} \Big|_{\bullet} &\approx \frac{u_{i+1,j,k} - u_{i,j,k}}{h_{x,i}^u}, & \frac{\partial v}{\partial y} \Big|_{\bullet} &\approx \frac{v_{i,j+1,k} - v_{i,j,k}}{h_{y,j}^v}, \\ \frac{\partial w}{\partial z} \Big|_{\bullet} &\approx \frac{w_{i,j,k+1} - w_{i,j,k}}{h_{z,k}^w}. \end{aligned} \quad (28)$$

The operator

$$\begin{aligned} \frac{1}{Re} (\nabla \cdot C[\mathbf{u}]) &= \frac{1}{Re} \left[ \frac{\partial^2(u^2)}{\partial x^2} + \frac{\partial^2(v^2)}{\partial y^2} + \frac{\partial^2(w^2)}{\partial z^2} \right. \\ &\quad \left. + 2 \frac{\partial(uv)}{\partial x \partial y} + 2 \frac{\partial(uw)}{\partial x \partial z} + 2 \frac{\partial(vw)}{\partial y \partial z} \right] \end{aligned} \quad (29)$$

is approximated in a similar way to those in Christov and Marinova (1998a). The functions  $u$ ,  $v$  and  $w$  in the approximation of the operator  $F$  are taken at the “old” time stage.

For the nonlinear terms we use an approximation with central differences which is akin to the ones proposed by Arakawa (1966) for the  $\psi - \omega$  formulation for ideal flows. A similar idea in primitive variables was elaborated in Marchuk (1982) with a special reference to the operator-splitting schemes

$$C_x^h[u] = \frac{u_{i+1/2,j,k}^n u_{i+1,j,k} - u_{i-1/2,j,k}^n u_{i-1,j,k}}{h_{x,i}^u + h_{x,i-1}^u}, \quad (30)$$

$$C_y^h[u] = \frac{v_{i-1/2,j+1,k}^n u_{i,j+1,k} - v_{i-1/2,j,k}^n u_{i,j-1,k}}{h_{y,j}^v + h_{y,j-1}^v}, \quad (31)$$

$$C_z^h[u] = \frac{w_{i-1/2,j,k+1}^n u_{i,j,k+1} - w_{i-1/2,j,k}^n u_{i,j,k-1}}{h_{z,k}^w + h_{z,k-1}^w}, \quad (32)$$

where  $u_{i+1/2,j,k}^n = (u_{i+1,j,k}^n + u_{i,j,k}^n)/2$ ,  $u_{i-1/2,j,k}^n = (u_{i,j,k}^n + u_{i-1,j,k}^n)/2$ , etc. The differences for nonlinear terms in the equations for  $v$  and  $w$  are similar to Eqs. (30)–(32).

This approximation is *conservative* in the sense that it is free of artificial scheme viscosity (diffusion) and hence the approximation of the nonlinear terms does not affect the evolution of the total energy of the process. Since the approximations of the nonlinear terms preserve their skew-symmetric property, the following statement is valid.

**THEOREM 1** Assume appropriate boundary conditions (homogenous, periodic, etc.) are imposed and the scalar product is

$$(\alpha, \beta) \stackrel{\text{def}}{=} \sum_{i,j,k} \alpha_{i,j,k} \beta_{i,j,k} \mathbf{h}_{x,i}^f \mathbf{h}_{y,j}^f \mathbf{h}_{z,k}^f, \quad (33)$$

where

$$\mathbf{h}_{x,i}^f = (h_{x,i}^f + h_{x,i-1}^f)/2, \quad \mathbf{h}_{y,j}^f = (h_{y,j}^f + h_{y,j-1}^f)/2, \quad \text{etc.}$$

and  $f = u, v, w$ , or  $p$ . Then the equalities hold

$$(C_x^h[u], u) = 0, \quad (C_y^h[u], u) = 0, \quad (C_z^h[u], u) = 0,$$

$$(C_x^h[v], v) = 0, \quad (C_y^h[v], v) = 0, \quad (C_z^h[v], v) = 0,$$

$$(C_x^h[w], w) = 0, \quad (C_y^h[w], w) = 0, \quad (C_z^h[w], w) = 0.$$

*Proof* It is sufficient to prove the first equality, namely  $(C_x^h[u], u) = 0$ . From the definition of  $C_x^h[u]$ , see Eq. (30), it follows that

$$\begin{aligned} (C_x^h[u], u) &= \sum_{i,j,k} u_{i,j,k} \frac{u_{i+1/2,j,k}^n u_{i+1,j,k} - u_{i-1/2,j,k}^n u_{i-1,j,k}}{h_{x,i}^u + h_{x,i-1}^u} \mathbf{h}_{x,i}^u \mathbf{h}_{y,j}^v \mathbf{h}_{z,k}^w \\ &= \frac{1}{2} \sum_{i,j,k} u_{i,j,k} \left( u_{i+1/2,j,k}^n u_{i+1,j,k} - u_{i-1/2,j,k}^n u_{i-1,j,k} \right) \mathbf{h}_{y,j}^v \mathbf{h}_{z,k}^w \\ &= \frac{1}{2} \sum_{j,k} \left[ u_{N_x,j,k}^n u_{N_x+1/2,j,k}^n u_{N_x+1,j,k} - u_{2,j,k}^n u_{1/2,j,k}^n u_{1,j,k} \right] \mathbf{h}_{y,j}^v \mathbf{h}_{z,k}^w. \end{aligned}$$

If we assume homogenous boundary conditions  $u|_{\partial\Omega} = 0$ , then  $u_{1/2,j,k} = u_{N_x+1/2,j,k} = 0$ . It follows immediately that  $(C_x^h[u], u) = 0$ .

The rest of the equalities can be proven in a similar way. The conservative approximations used here alleviate the problem of artificial viscosity as far as the steady-state solution is concerned. No terms proportional to the second derivatives (artificial viscosity/diffusivity) are present for the approximation of the steady-state case after the time steps (iterations) *converge*.

**ALGORITHM FOR SOLVING THE DISCRETE PROBLEM**

After the discretization for each time step we have obtained a linear algebraic system. The scheme described above allows a very efficient treatment of the algebraic systems. One of the systems for the respective velocity component is always conjugated to the system for the pressure set function. For instance, on the first time stage the  $x$  operators are inverted along the line  $y = y_j, z = z_k$  when  $u$  and  $p$  are conjugated. Therefore, three (or two in the 2D case) linear algebraic systems are solved: two for the set functions

$$\mathbf{v}^{n+1/3} = \text{column} \left[ v_{1,j,k}^{n+1/3}, \dots, v_{i,j,k}^{n+1/3}, \dots, v_{N_x,j,k}^{n+1/3} \right]$$

and

$$\mathbf{w}^{n+1/3} = \text{column} \left[ w_{1,j,k}^{n+1/3}, \dots, w_{i,j,k}^{n+1/3}, \dots, w_{N_x,j,k}^{n+1/3} \right]$$

with tridiagonal matrices (for definiteness, call them  $\mathcal{A}_v$  and  $\mathcal{A}_w$ ), and another (a conjugated one) – for

the “composite” difference function

$$(\mathbf{up})^{n+1/3} = \text{column} \left[ \begin{matrix} u_{1,j,k}^{n+1/3}, p_{1,j,k}^{n+1/3}, \dots, u_{i,j,k}^{n+1/3}, p_{i,j,k}^{n+1/3}, \dots, \\ p_{N_x,j,k}^{n+1/3}, u_{N_x+1,j,k}^{n+1/3} \end{matrix} \right]$$

which turns out to be a pentadiagonal matrix twice the size of the tridiagonal ones (call it  $\mathcal{A}_{up}$  for definiteness). Thus the following linear algebraic systems are solved for the selected  $y = y_j, z = z_k$  :

$$\begin{aligned} \mathcal{A}_{up} \cdot (\mathbf{up})^{n+1/3} &= \mathcal{B}_{up}, & \mathcal{A}_v \cdot \mathbf{v}^{n+1/3} &= \mathcal{B}_v, \\ \mathcal{A}_w \cdot \mathbf{w}^{n+1/3} &= \mathcal{B}_w. \end{aligned} \tag{34}$$

In the same manner, the second and the third half-time steps require to solve the following algebraic systems

$$\begin{aligned} \mathcal{B}_u \cdot \mathbf{u}^{n+2/3} &= \mathcal{S}_u, & \mathcal{B}_{vp} \cdot (\mathbf{vp})^{n+2/3} &= \mathcal{S}_{vp}, \\ \mathcal{B}_w \cdot \mathbf{w}^{n+2/3} &= \mathcal{S}_w \end{aligned} \tag{35}$$

and

$$\begin{aligned} \mathcal{D}_u \cdot \mathbf{u}^{n+1} &= \mathcal{T}_u, & \mathcal{D}_v \cdot \mathbf{v}^{n+1} &= \mathcal{T}_v, \\ \mathcal{D}_{wp} \cdot (\mathbf{wp})^{n+1} &= \mathcal{T}_{wp}. \end{aligned} \tag{36}$$

The general sequence of the algorithm for solving the discrete problem is as follows.

- (i) Set values of the parameters  $Re, \tau, N_x, N_y, N_z$ , and the initial guess  $\mathbf{u}_{i,j,k}^0, p_{i,j,k}^0$ .
- (ii) Calculate the values  $\mathbf{u}_{i,j,k}^{n+1/3}, p_{i,j,k}^{n+1/3}$  from Eq. (34) for the first step considering  $\mathbf{u}_{i,j,k}^n, p_{i,j,k}^n$  as known.
- (iii) Calculate the values  $\mathbf{u}_{i,j,k}^{n+2/3}, p_{i,j,k}^{n+2/3}$  from Eq. (35) for the second step using  $\mathbf{u}_{i,j,k}^n, p_{i,j,k}^n$  and  $\mathbf{u}_{i,j,k}^{n+1/3}, p_{i,j,k}^{n+1/3}$ .
- (iv) Calculate the values  $\mathbf{u}_{i,j,k}^{n+1}, p_{i,j,k}^{n+1}$  from Eq. (36) for the third step using  $\mathbf{u}_{i,j,k}^n, p_{i,j,k}^n$  and  $\mathbf{u}_{i,j,k}^{n+2/3}, p_{i,j,k}^{n+2/3}$ . Set the pressure  $p_{i,j,k}^{n+1} := p_{i,j,k}^{n+1} - \hat{p}^{n+1}$ , where  $\hat{p}^{n+1}$  is the average of the pressure.
- (v) If the following criterion is satisfied

$$\begin{aligned} \max\{R^u(n), R^v(n), R^w(n), R^p(n)\} &\leq \varepsilon, \\ \text{where } R^f(n) &\stackrel{\text{def}}{=} \frac{\max_{i,j,k} |f_{i,j,k}^{n+1} - f_{i,j,k}^n|}{\tau \max_{i,j,k} |f_{i,j,k}^{n+1}|} \end{aligned} \tag{37}$$

then the calculation is terminated. Otherwise the index of iterations is stepped up  $n := n + 1$  and the algorithm is returned to step (ii).

We solve the multidagonal systems by means of a specialized Gaussian-elimination solver Christov (1994) employing pivoting which is a generalization of what in

the tridiagonal case is called *Thomas algorithm* in the English-language literature or “progonka” in the Russian-language literature. Any other solver will do the job too. The specialized one is somewhat faster for the systems under consideration whose number of diagonals is rather small. The algorithm for solving the difference equations is easy to vectorize—the sequence of one-dimensional problems (five- and three- diagonal systems) at each time step can be solved in a parallel manner.

### NUMERICAL RESULTS

To verify the practical properties of the new scheme, we conduct different numerical tests. In order to demonstrate the second-order rate of convergence and no dependence of the numerical solution on the time increment, a test with 3D analytic solution is done. Next, we present a numerical solution for the 2D lid-driven flow in cavities with different aspect ratios. Our purpose is to obtain accurate stationary solutions for these flows for Reynolds numbers as high as possible using very fine grids. In the end we treat the flow after a backward-facing step using a non-uniform grid. The admissible tolerance is chosen to be  $\varepsilon \leq 10^{-10}$  for the criterion of convergence (37). The initial guess is taken to be zero unless otherwise specified.

### Scheme Validation

Tests with analytic solutions are done in order to demonstrate that the difference scheme has second-order rate of convergence if a uniform grid is used and independence of steady state solution on time step increment  $\tau$ . The Navier–Stokes equations are solved in

$$\Omega = \{0 \leq x \leq 1, 0 \leq y \leq 1, 0 \leq z \leq 1\}$$

on a uniform grid by using the following solution

$$\begin{aligned} \mathbf{u} &= \begin{pmatrix} u \\ v \\ w \end{pmatrix} = \begin{pmatrix} \sqrt{2} \exp(-\sqrt{2}x) \cos(y+z) \\ \exp(-\sqrt{2}x) \sin(y+z) \\ \exp(-\sqrt{2}x) \sin(y+z) \end{pmatrix}, \\ p &= -\exp(-2\sqrt{2}x). \end{aligned} \tag{38}$$

We employ respective boundary conditions only for the velocity components  $u, v$  and  $w$  and do not impose any boundary condition for pressure  $p$ .

Since the problem has an analytic solution, we can calculate the error in the numerical solution directly. The following maximum and average errors are used as a measure:

$$\begin{aligned} \text{Error}_{f,\max} &= \max_{i,j,k} |f_{i,j,k}^{\text{num.}} - f_{i,j,k}^{\text{anal.}}|, \\ \text{Error}_{f,\text{aver.}} &= \sum_{i,j,k} \frac{|f_{i,j,k}^{\text{num.}} - f_{i,j,k}^{\text{anal.}}|}{N_x N_y N_z}, \end{aligned} \tag{39}$$

where  $f$  stands for one of the functions  $u, v, w$  or  $p$ .

The numerical solutions are obtained by iterating until the norms  $R^u(n), R^v(n), R^w(n)$  and  $R^p(n)$  became

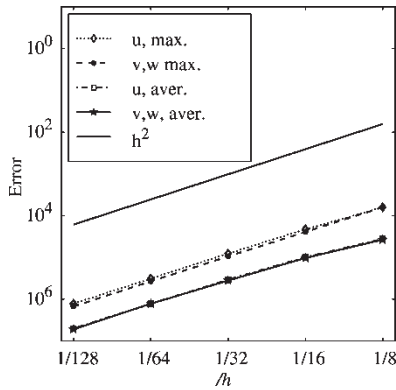


FIGURE 1 Discretization error as a function of the mesh spacing  $h = h_x = h_y = h_z$ .

negligibly small (of order of the round-off error in double precision). The exact maximum and average discretization errors for  $u$ ,  $v$  and  $w$  are presented in Figs. 1 and 2 for  $Re = 10$ . Fig. 1 shows the error for different grid spacings  $h_x = h_y = h_z = h = 1/128, 1/64, 1/32, 1/16, 1/8$  and  $h^2$ . It is readily seen that the error of the numerical solution is of second order. The difference between numerical and analytic pressure is equal to the constant. Since in the analytic solution  $v = w$ , the exact errors in the numerical solutions for these velocity components are practically identical (undistinguished on the figure).

As has been already mentioned, the solution of the stabilizing correction scheme does not depend on the time increment  $\tau$ , see Eq. (19). The difference scheme is tested for independence on the time increment by calculations with different values of  $\tau$  in the interval  $[0.001, 1]$ . The results presented in Fig. 2 confirm the full approximation of the scheme (no dependence of the steady-state solution on the magnitude of time increment  $\tau$ ).

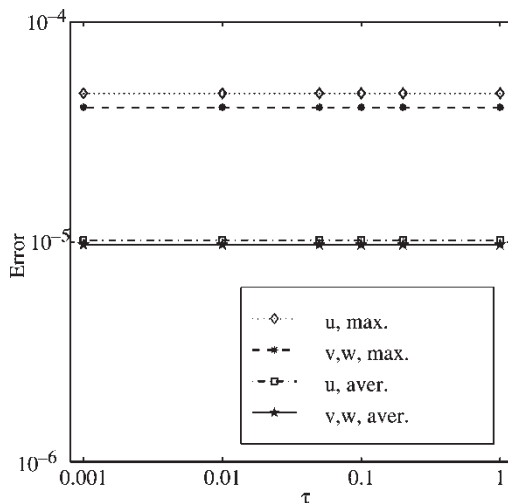


FIGURE 2 Discretization error as a function of the time increment  $\tau$ ,  $h = 1/16$ .

## Cavity Flow

Consider the well-known lid-driven cavity problem. Driven cavity flow has usually been a standard case study for any new scheme for Navier–Stokes equations. Published results are available for this flow problem from a numbers of sources – for solutions at high Reynolds numbers, see Ghia *et al.* (1982), Kim and Moin (1985) and Bruneau and Jouron (1990) among many others.

The flow occupies the region  $\Omega = \{0 \leq x \leq a, 0 \leq y \leq b\}$ . In our formulation the boundary conditions for the lid-driven cavity flow read

$$\begin{aligned} u(x, 0) = u(0, y) = u(a, y) = 0, \quad u(x, b) = 1, \\ v(x, 0) = v(x, b) = v(0, y) = v(a, y) = 0, \end{aligned} \quad (40)$$

$$\left. \frac{\partial u}{\partial x} \right|_{(0,y)} = \left. \frac{\partial u}{\partial x} \right|_{(a,y)} = \left. \frac{\partial v}{\partial y} \right|_{(x,0)} = \left. \frac{\partial v}{\partial y} \right|_{(x,b)} = 0. \quad (41)$$

### Flow in a Square Cavity ( $a = b$ )

By now a consensus has almost been reached that for the real physical flow a non-steady regime takes place for  $Re > 10\,000$ . It was obtained that the numerical solution of the steady-state Navier–Stokes equations exists for  $Re \leq 11\,000$ . High accurate results were obtained using uniform grids with spacings  $1/h = 256$ ,  $1/h = 512$ , and Richardson extrapolation from these solutions. For Reynolds numbers greater than 11 000 we were unable to get convergence with the above fine uniform grids.

For large Reynolds numbers we observe the onset of oscillations much in the fashion as reported in Shen (1991) where a Hopf bifurcation was observed for the real-time system. As already mentioned in the section “Evolution System”, the dynamical properties of our system are of no physical interest and we did not examine in detail the bifurcation and transition to an unsteady/unstable regime.

The boundary conditions in Shen (1991) avoid the problem of discontinuity of the longitudinal component of velocity in the points where the lid touches the vertical walls. In this sense the relevance of the results from Shen (1991) to the classical lid-driven flow should be understood in a qualitative sense. On the other hand in a recent paper, Shankar and Deshpande (2000), the authors claim the following: “There is some computational evidence that the field becomes unsteady around  $Re = 13\,000$ . If the flow does become unsteady, what is the nature of this flow, because it cannot, as a 2-D flow, be turbulent? Are there steady solutions that cannot be computed because they are unstable? Although these are natural questions, they are not of practical relevance, because, as we show below, 2-D flows are almost fictitious.”

This said, we are aware that the steady solutions for  $Re \geq 7500$  (if we choose to side with Shen (1991)) or  $Re \geq 13\,000$  (if we adopt the assessment from Shankar and Deshpande (2000)) might never be encountered in

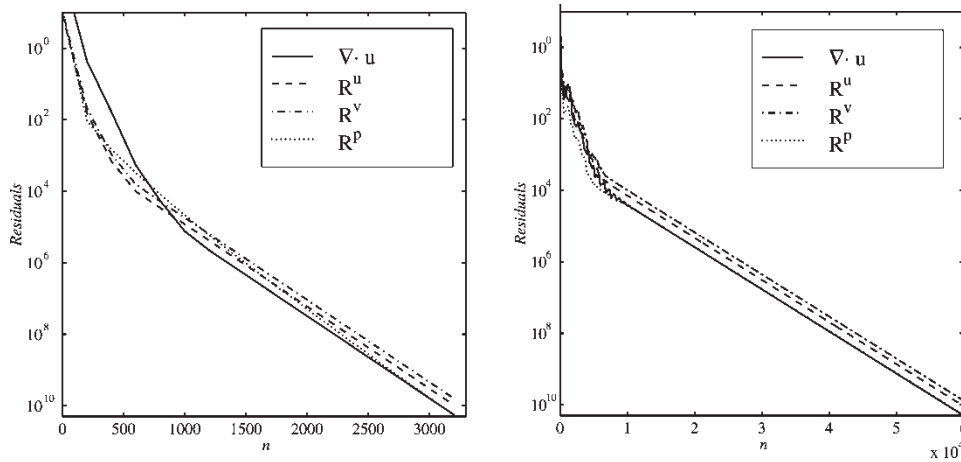


FIGURE 3 The rate of convergence with the number of iteration of the residuals  $R^u, R^v, R^p$  in  $L_1$  norm as well as the divergence  $\nabla \cdot \mathbf{u}$  for  $h = 1/512$ . Left panel:  $Re = 1000$ . Right panel:  $Re = 10000$ .

a physical flow with a standard level of external perturbations. Yet the steady patterns obtained here are valid solutions of the steady-state Navier–Stokes equations and it is of interest to have them on record as a signature of the flow itself.

Figure 3 shows the convergence of the iterations for two different Reynolds numbers. The uniform norms of the residuals of the equations for  $u, v$  and  $p$ , as well as of  $\nabla \cdot \mathbf{u}$ , are plotted versus the number of iterations. Clearly, all of these residuals approach zero exponentially.

The accurate calculation of the magnitudes and locations of the centers of the primary, secondary and tertiary vortices is one of the hardest tests. The calculated location of the center of the primary vortex as a function of the Reynolds number is shown in Fig. 4 and compared to some of the literature sources. It is clearly seen that our

curve is self-consistent and monotone while the literature data are more scattered. An interesting observation is that the scheme of Schreiber and Keller (1983), which is off up to 30% for the amplitude of the stream function, gives relatively good predictions for the centers. This means that our scheme not only lacks artificial viscosity but also has very low phase error. When it comes to these fine-structure characteristics even the overall accurate results of many of the literature works are subject to these difficulties stemming from the artificial dispersion.

It should be mentioned here that the last property is not obvious and cannot be proven strictly for a nonlinear scheme. On the other hand, the artificial scheme dispersion can be very detrimental for the speed of convergence of the method and can also create spatial wiggles in the steady-state solution.

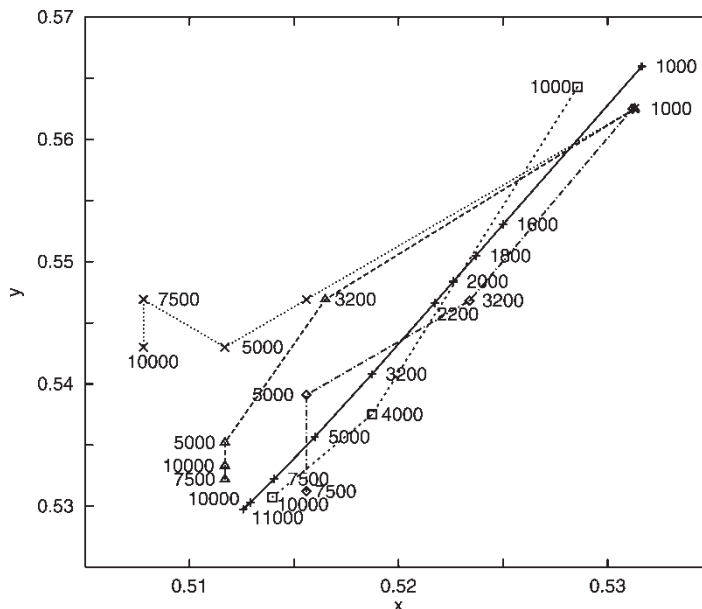


FIGURE 4 Effect of  $Re$  on the location of vortex centers: — + — present results;  $\Delta$  Ghia *et al.* (1982) for  $Re = 1000, 3200, 5000, 7500, 10000$ ;  $\square$  Schreiber and Keller (1983) for  $Re = 1000, 4000, 10000$ ;  $\times$  Liao and Zhu (1996). Primary vortex.

Downloaded by [Christo Christov] at 20:15 13 October 2011

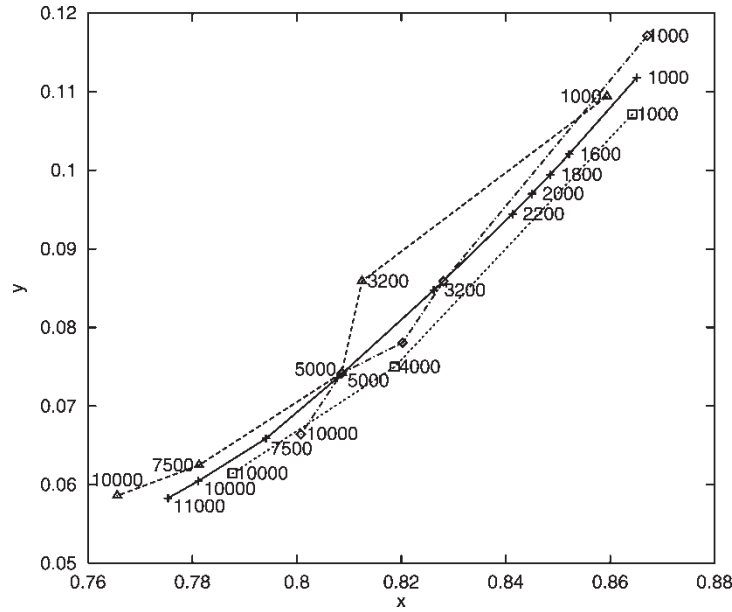


FIGURE 5 Effect of  $Re$  on the location of vortex centers: — + — present results;  $\Delta$  Ghia *et al.* (1982) for  $Re = 1000, 3200, 5000, 7500, 10000$ ;  $\square$  Schreiber and Keller (1983) for  $Re = 1000, 4000, 10000$ ;  $\times$  Liao and Zhu (1996). Bottom-right secondary vortex.

The scenario of appearance of the secondary and the tertiary vortices is qualitatively well established in the literature. The vortex in the bottom right corner first appears for  $Re \approx 100$ . The bottom left corner is occupied by another secondary vortex for  $Re \approx 400$  and it remains less intensive than the bottom right vortex for all Reynolds numbers. With the increase of  $Re$  the center of the primary vortex shifts towards the geometric center of the cavity. This kind of behavior is connected with the development of an inviscid core of the flow and boundary layers near the walls. As shown in Fig. 5, the position of the bottom right vortex is also a function of the Reynolds number. Its center shifts to the central vertical cross-section with the increase of  $Re$ .

Table I summarizes the data concerning the location and strengths of the primary vortex and the most significant secondary vortex in the bottom right corner. The thorough comparison for the different flow characteristics as obtained in different works from the literature can be found in a previous authors' work (Christov and Marinova (2001)). Here, we concentrate on the issue of the

equivalence between the formulation involving the Poisson equation for pressure (1), (8) and the original formulation of the incompressible Navier–Stokes Eqs. (1), (2).

It is seen in Fig. 6 that the divergence  $\nabla \cdot \mathbf{u}$  is of order of  $10^{-11}$  in the whole region. This is true even near the corner points of velocity discontinuity where the lid touches the vertical walls, the divergence is very small. In the light of the estimates from Kangro and Nicolaides (1999), the present result means that the uniform grid (even though very dense) has a smoothing effect upon the discontinuity of the velocity components and the divergence as well.

The apparent equivalence of the *difference* approximations of the two formulations is due to the fact that when a discontinuity is present in a corner point of the boundary it presents usually a lesser singularity than in a regular point of the smooth part of the boundary. It means that the derivatives of the sought functions are power functions of the distance from the corner with a weaker singularity. Naturally the uniform grid smoothes these singularities in the immediate points adjacent to

TABLE I Coordinates of the extrema of the stream function, square cavity

$Re$	$1/h$	Primary vortex		Right-bottom vortex	
		$\psi_{\min}$	$(x_{\min}, y_{\min})$	$\psi_{\max}$	$(x_{\max}, y_{\max})$
1000	512	-0.116269	(0.5316, 0.5660)	0.001640	(0.8651, 0.1118)
	R 256	-0.116915	(0.5313, 0.5664)	0.001666	(0.8672, 0.1133)
3200	512	-0.116410	(0.5187, 0.5408)	0.002676	(0.8262, 0.0847)
	R 256	-0.119257	(0.5195, 0.5391)	0.002726	(0.8281, 0.0859)
5000	512	-0.116120	(0.5160, 0.5357)	0.002890	(0.8077, 0.0736)
	R 256	-0.118047	(0.5156, 0.5352)	0.002940	(0.8086, 0.0742)
10000	512	-0.113848	(0.5129, 0.5303)	0.003010	(0.7812, 0.0605)
	R 256	-0.116470	(0.5125, 0.5302)	0.003050	(0.7787, 0.0602)
11000	512	-0.113394	(0.5126, 0.5298)	0.002977	(0.7754, 0.0583)

R – Richardson extrapolation from solutions  $256 \times 512$  and  $512 \times 1024$ .

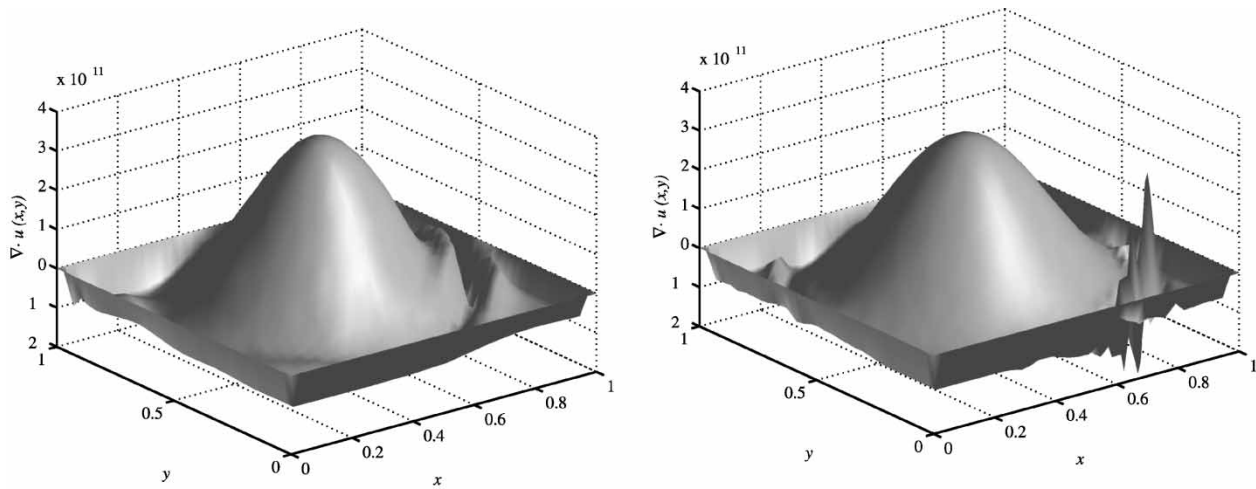


FIGURE 6 The pointwise distribution of  $\nabla \cdot u$  for  $h = 1/512$ . Left panel:  $Re = 1000$ ,  $\tau = 0.09$ . Right panel:  $Re = 10000$ ,  $\tau = 0.05$ .

the boundary points. Some preliminary experiments with nonuniform grids suggest that a singularity in  $\nabla \cdot \mathbf{u}$  can be expected to develop (as pointed out in Kangro and Nicolaides (1999)) if the nonuniform mesh changes very rapidly near the corner points. However, it takes a special investigation which will be done elsewhere.

#### Flow in a Deep Cavity (Aspect Ratio 2)

The flow regime is more complex for deeper cavities. Alongside the Reynolds number  $Re$ , the aspect ratio  $A = b/a$  enters as a second bifurcation parameter. We consider a rectangular cavity with aspect ratio  $A = 2$ . In Goodrich *et al.* (1990) periodic solutions are found for  $Re = 5000$ . Steady solutions are obtained in Bruneau and Jouron (1990) and Goyon (1996). The comparisons provided in Bruneau and Jouron (1990) for the problems in the square driven cavity and in a rectangular one of aspect ratio 2 shows that the first signs of instability, occurring in the square cavity for  $Re > 5000$ , can appear as early as for  $Re = 1000$  in the rectangular one. Clearly, the latter flow is more unstable than the former. Our aim is to show that the *iterative* scheme is able to determine steady-state solutions for high Reynolds numbers. Once again, we are to point out that one should not compare the temporal dynamics of real-time schemes of the type of Bruneau and Jouron (1990) to the dynamics of a fictitious-time (iterative) scheme of the type presented here. The iterative scheme can converge for Reynolds numbers much larger than the physically admissible values. The results for high  $Re$  are presented here not as a novel physical result about the onset of instability, but rather for the sake of understanding the numerical aspects of the algorithm.

We use uniform grids with spacings  $h = h_x = h_y = 1/64, 1/128, 1/256, 1/512$ . The rate of approaching the steady solution depends on the time step increment  $\tau$ . The optimal value of  $\tau$  is found from the numerical experiments to be  $\tau = 0.09$ .

We conducted numerical calculations for this problem up to  $Re = 6000$  and have obtained steady solutions with

all grids starting from zero initial guess. Since we employ primitive variables the most natural characteristics to present are the velocity components. The numerical results with different uniform grids with  $Re = 1000$  are in close agreement. The results clearly demonstrate that the discretization error is of  $O(N_x^{-2} + N_y^{-2})$ .

The streamlines obtained using Richardson extrapolation from the solutions on uniform grids with  $h = 1/256$  and  $h = 1/512$  for  $Re = 1000, 3200$  and  $6000$ , are presented in Fig. 7. There is a significant difference between our results and the results in Bruneau and Jouron (1990) in the lower part of the cavity. It is probably due to the presence of instabilities during iterations in Bruneau and Jouron (1990). The lower right and left second vortices are more intensive in our work compared with Goyon (1996).

The data concerning the location and strengths of the top primary vortex and the bottom primary vortex are presented in Table II. Our results for  $Re = 1000$  are compared with Bruneau and Jouron (1990) and Goyon (1996) ( $256 \times 512$  grid cells). There is good agreement between our results and Bruneau and Jouron (1990) for  $\psi_{\min}$ , while for  $\psi_{\max}$  the computational results in Goyon (1996) are close to ours—the difference is less about 1%. Whereas, the difference with Bruneau and Jouron (1990) for the value of  $\psi_{\max}$  is greater than 10%. For Reynolds number  $Re > 1000$  we were unable to find in the literature steady-state solution data for comparisons. Therefore, we present only our results obtained with  $h = 1/256, 1/512$  and the Richardson extrapolation from these solutions.

#### Flow Over a Backward-facing Step in a Channel

Consider the flow over a backward-facing step, which is another well-studied test case. Figure 8 shows the geometry of the flow and the defined flow parameters. Experimental results for this flow are presented in Armaly *et al.* (1983) and numerical results can be found in a number of papers (Gartling, 1990; Gresho *et al.*, 1993; Barton, 1997;

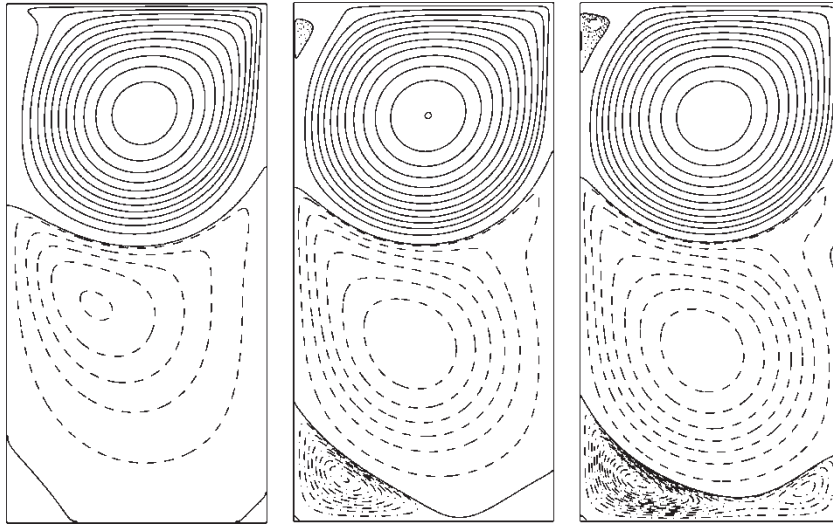


FIGURE 7 Streamlines for different Reynolds numbers. Contour values: — starting from zero with increment  $-0.01$ ; --- starting from  $+0.001$  with increment  $+0.003$ ; - - - starting from  $-0.00002$  with increment  $-0.00004$ ; ··· starting from  $+0.0001$ , with increment  $+0.0001$ .

Keskar and Lyn, 1999). The Reynolds number  $Re = UH/\nu$  is based on the mean inflow velocity  $U$ , the channel height  $H$ , and the viscosity  $\nu$ . The experimental results of Armaly *et al.* (1983) indicate that the three-dimensional effects appear for  $Re > 400$  and the measurements and theoretical prediction begin to deviate from each other after that Reynolds number. The fact that the solution of the incompressible Navier–Stokes equations over a backward-facing step at  $Re = 800$  is steady and stable has been confirmed in a number of recent works, see, for example, Gartling (1990), Gresho *et al.* (1993), Barton (1997) and Keskar and Lyn (1999), where accurate steady-state numerical solutions have been obtained up to  $Re = 800$ .

### Definition of Problem Parameters

We impose non-slip boundary conditions on the walls of the channel. At the inflow boundary ( $x = 0, h \leq y \leq H$ ) a parabolic profile  $u = 6U(H - y)(y - h)/(H - h)^2$ ,  $v = 0$  is prescribed. The outflow velocity profile is also taken to be parabolic  $u = 6U(H - y)y/H^2$ ,  $v = 0$ . The ratio

between the height of the step  $h$  and the height of the channel  $H$  is taken to be  $h : H = 1 : 2$ .

We chose a non-uniform grid. Three different grid sizes are used in the computations. The numbers of cells for the coarsest grid (Grid 1) are  $N_x = 256$  and  $N_y = 64$ , respectively. The grid is dense near the walls, while in direction  $x$  near the outlet boundary the grid is much coarser. In the interval  $[0, x_c]$ , where  $x_c$  is such that  $x_c > x_{TR}$ , a fine regular grid is employed with a number of grid cells  $N_c$ . Because in the interval  $[x_c, x_L]$  the flow is almost uniform, less numbers of grid cells are used which are distributed as follows

$$x_i = x_L - (x_L - x_c) \frac{\tanh(f_x \xi_i)}{\tanh(f)},$$

$$\text{where } \xi_i = 1 - \frac{i - N_c - 1}{N_y - N_c - 1},$$

$$i = -N_c + 1, \dots, N_y.$$

TABLE II Positions of the stream function extrema for the cavity with aspect ratio 2

$Re$	Ref. data	$1/h$	Primary top vortex		Primary bottom vortex	
			$\psi_{\min}$	$(x_{\min}, y_{\min})$	$\psi_{\max}$	$(x_{\max}, y_{\max})$
1000	Bruneau and Jouron (1990)	256	-0.1169	(0.5273, 1.5625)	0.0148	(0.3516, 0.7891)
	Goyon (1996)	256	-0.1187	(0.5313, 1.5781)	0.0132	(0.3359, 0.8476)
	Present work	256	-0.114547	(0.5309, 1.5791)	0.012763	(0.3423, 0.8373)
	Present work	512	-0.117095	(0.5302, 1.5794)	0.013119	(0.3423, 0.8378)
3200	Present work	R256	-0.117945	(0.5299, 1.5795)	0.013330	(0.3424, 0.8379)
	Present work	256	-0.113984	(0.5183, 1.5625)	0.017716	(0.4489, 0.6829)
	Present work	512	-0.118552	(0.5177, 1.5643)	0.018580	(0.4505, 0.6857)
	Present work	R256	-0.120075	(0.5175, 1.5648)	0.018869	(0.4510, 0.6866)
6000	Present work	256	-0.111564	(0.5154, 1.5605)	0.019809	(0.4687, 0.6493)
	Present work	512	-0.117709	(0.5148, 1.5636)	0.021013	(0.4692, 0.6584)
	Present work	R256	-0.119759	(0.5147, 1.5645)	0.021418	(0.4694, 0.6612)

R – Richardson extrapolation from solutions  $256 \times 512$  and  $512 \times 1024$ .

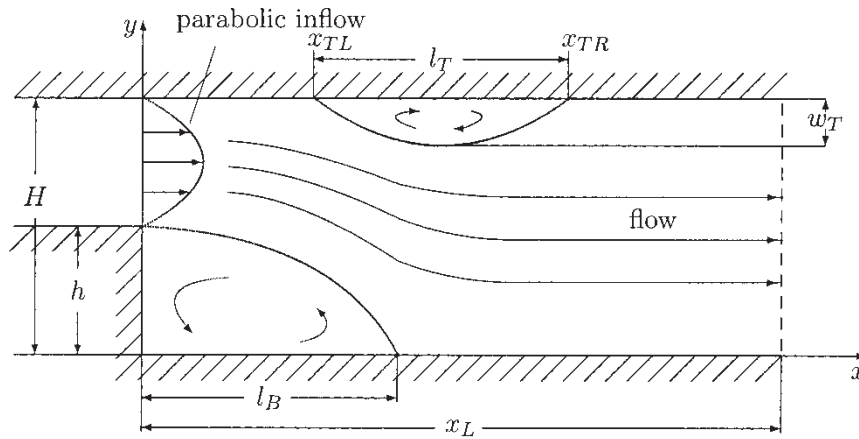


FIGURE 8 Geometry of the flow over a backward-facing step in a channel ( $h : H = 1 : 2$ ).

In direction  $y$  the mesh is defined in a similar fashion, namely

$$y_j = h \left\{ 1 + \frac{\tanh[\xi_j - h]f_y}{\tanh(hf)} \right\}, \quad \text{where } h = \frac{H}{2},$$

$$\xi_j = \frac{(j-1)H}{N_y - 1}, \quad j = 1, \dots, N_y.$$

Here we select  $f_x = 2.28$  and  $f_y = 4$ , respectively.

The finer grid (Grid 2) is constructed on the base of the coarse Grid 1 by adding a middle point between two grid points. The finest grid (Grid 3) is constructed on the base of Grid 2. Finally, using the obtained solutions on the last two grids, Richardson extrapolation is performed to increase the accuracy of the solutions to fourth order. We mention here that on a non-uniform grid the second order of the approximations of the derivatives is locally proportional to the larger spacing. More specifically the order is  $O(h_i - h_{i+1})$  which is second order with respect to the larger spacing provided that the grid depends smoothly enough on the spatial variables. For this reason after applying Richardson extrapolation, we get in practice an overall approximation which is slightly worse than fourth order.

### Stability and Accuracy

Our tests have shown that for  $Re \leq 1250$  it is safe to take  $x_L \approx 100h$ . However, for  $Re \geq 1275$  a “longer” channel has to be used (for example  $x_L = 140h$ ), because of the appearance of instabilities in the numerical solution on our coarsest grid for some value of Reynolds number in the interval (1250,1275).

On the finer grids, the numerical scheme is stable for  $Re = 1550$  on all grids and  $x_L = 140h$  despite the long oscillation on Grid 1 in the beginning of the iterative process. Convergence is reached for arbitrary initial conditions, but it is much faster if the converged solution for a neighboring Reynolds number is used as initial condition. Some of our computations are performed using as initial condition the solution for the previous smaller  $Re$ .

To test the accuracy of the scheme for this problem we compare our numerical results for  $Re = 800$  on different grids with accurate benchmarks from the literature (Gartling, 1990; Gresho *et al.*, 1993; Barton, 1997; Keskar and Lyn, 1999). The most representative characteristics of the flow over a backward-facing step are the reattachment lengths  $l_B$  and  $l_T$  because of their dependence on the Reynolds number. In Table III the values of reattachment lengths  $l_B$ ,  $l_T$ , and the values of upper eddy start,  $x_{TL}$  and upper eddy end,  $x_{TR}$  are presented.

TABLE III Comparison of present results (Richardson extrapolation from the solutions with Grid 2 and Grid 3) on characteristic flow parameters with results from the literature for  $Re = 800$

Work	$l_B$	$l_T$	$x_{TL}$	$x_{TR}$	$\psi_{\min}$	$\psi_{\max}$	Nodes
Barton (1997)	6.015	5.66	4.82	10.48			
Gartling (1990)	6.10	5.63	4.85	10.48	-0.0342	0.5064	129681
Gresho <i>et al.</i> (1993) FD	6.082	5.6260	4.8388	10.4648	-0.034195	0.50661	245760
Gresho <i>et al.</i> (1993) SE	6.10	5.63	4.86	10.49	-0.0342	0.5065	$\geq 8000$
Keskar and Lyn (1999)	6.0964	5.6251	4.8534	10.4785	-0.03420	0.50653	3737
Present	6.0909	5.6505	4.8214	10.4719	-0.03421	0.50653	Extr.

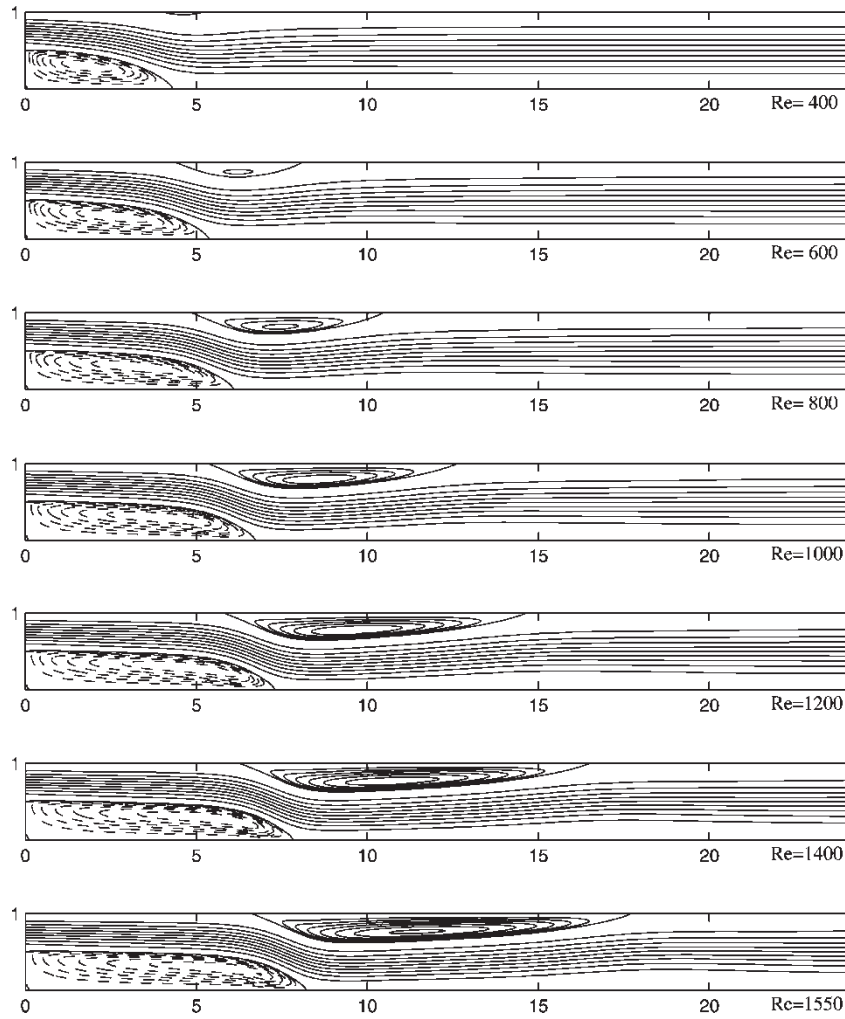


FIGURE 9 Streamlines for different  $Re$  (expansion ratio 1:3). Contour values are:  $-0.035, -0.030, -0.025, -0.020, -0.015, -0.010, -0.005, 0.0, 0.05, 0.15, 0.20, 0.25, 0.30, 0.35, 0.40, 0.45, 0.50, 0.502, 0.504, 0.506, 0.508, 0.510, 0.512$ .

### Flow Characteristics

We have calculated stationary solutions for this flow for values of Reynolds number in the interval  $Re \in [10, 1550]$ . All computations are performed with  $\tau = 0.1$ . Figure 9 shows the streamline plots for Reynolds numbers 400, 600, 800, 1000, 1200, 1400 and 1550. At  $Re = 400$  the secondary eddy is weak but clearly visible on the upper wall of the channel, see also Thompson and Ferziger (1989). For higher Reynolds numbers the secondary eddy is longer and stronger.

The most representative characteristics of the flow as a function of the Reynolds number are shown in Fig. 10 and Table IV. Our results for the length  $l_B$  are similar to those in Kim and Moin (1985) for Reynolds numbers up to 800. Both our results and those of Armaly *et al.* (1983) and Kim and Moin (1985) deviate from the experimental values of Armaly *et al.* (1983). According to Armaly *et al.* (1983) and Kim and Moin (1985) the differences between the experimental

and computational results are not a result of numerical errors. The difference is due to the three-dimensionality of the experimental flow at  $Re = 800$ . In our calculations (up to  $Re = 1550$ ) we observe that the appearance of the upper eddy (for the value of  $Re \gtrsim 400$ ) slows down the growth of the bottom eddy, see Fig. 10(a). For Reynolds number  $Re \geq 600$  the dependence of the reattachment length  $l_B$  on  $Re$  is almost linear with a smaller slope than that for  $Re \leq 400$ . The upper eddy  $l_T$  grows faster than  $l_B$ . For a certain value of  $Re \lesssim 900$  the length  $l_T$  becomes longer than the length of the bottom eddy  $l_B$ . Figure 10(b) shows the dependence of the width of the secondary eddy  $w_T$  on the Reynolds number.

### CONCLUSION

The main advantages of the new splitting scheme can be summarized as follows: it is applicable for

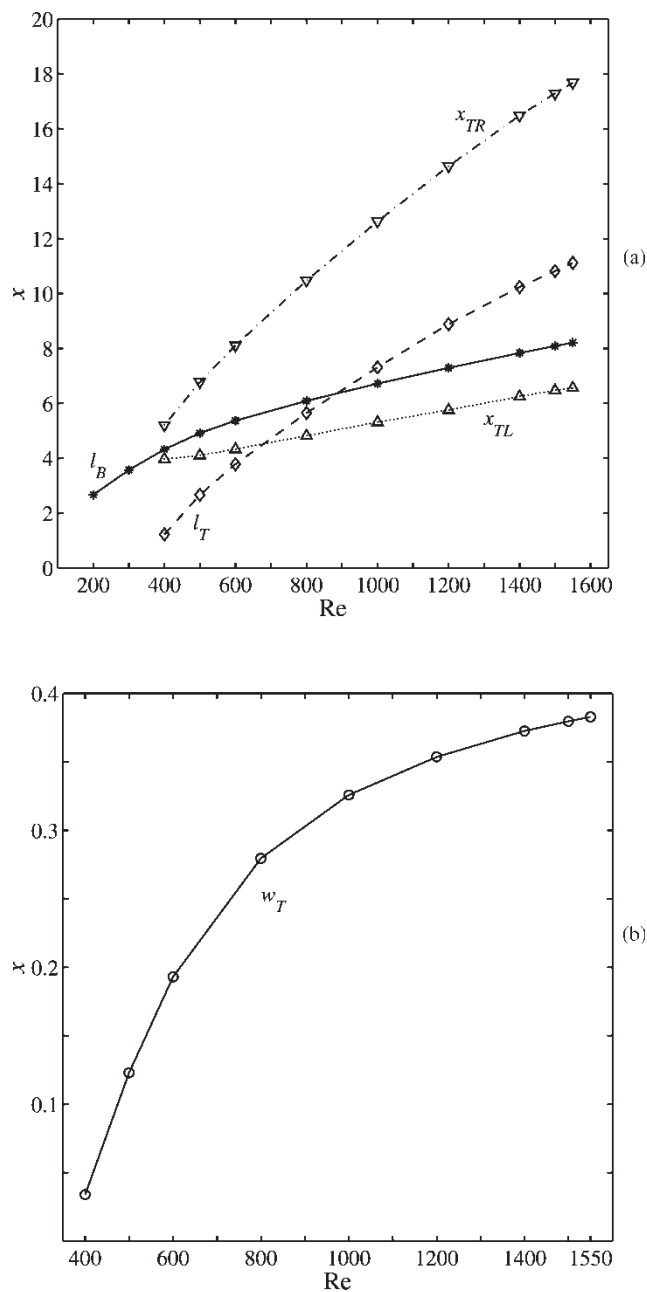


FIGURE 10 Variation in different flow characteristics with Reynolds number: (a) reattachment and separation lengths ( $*$  -  $l_B$ ;  $\diamond$  -  $l_T$ ;  $\triangle$  -  $x_{TL}$ ;  $\nabla$  -  $x_{TR}$ ); (b) width  $w_T$  of the upper eddy.

solving three-dimensional steady incompressible flows. The scheme possesses second-order accuracy (no artificial viscosity) and the approximation of nonlinear terms is conservative on Cartesian grids. The coordinate splitting reduces the computational time per time step/iteration in orders of magnitude in comparison with the implicit schemes employing inversion of the non-split operators. Therefore the algorithm proposed here is very efficient for solving large-scale problems. The method exhibits a strong stability for solving steady flows at large Reynolds numbers using fine grid spacings. Accurate stationary solutions are obtained for

the problems under consideration for a range of Reynolds numbers which significantly exceeds the literature.

#### Acknowledgements

The support for R. Marinova from the Japan Science and Technology Agency under STA Fellowship ID No.200131 is gratefully acknowledged. The work of C. Christov is supported by Grant LEQSF (1999-02)-RD-A-49 from the Louisiana Board of Regents.

TABLE IV Characteristic flow parameters for different values of  $Re$ :  $Re_l$  – results with long channel  $x_L = 140h$ ;  $\psi_{\min}$ ,  $\psi_{\max}$ ,  $(x_{bv}, y_{bv})$ , and  $(x_{tv}, y_{tv})$  are the minimum and maximum and its locations of stream function

$Re$	$l_B$	$l_T$	$x_{TL}$	$x_{TR}$	$w_T$	$\psi_{\min}(x_{bv}, y_{bv})$	$\psi_{\max}(x_{tv}, y_{tv})$
400	4.3223	1.2286	3.9732	5.2018	0.0340	-0.034023 (1.7999, 0.2992)	0.500014 (4.6116, 0.9774)
600	5.3703	3.7816	4.3304	8.1119	0.1930	-0.034185 (2.6083, 0.2978)	0.502321 (6.2166, 0.8715)
800	6.0909	5.6505	4.8214	10.4719	0.2796	-0.034210 (3.4000, 0.2955)	0.506533 (7.4507, 0.8154)
1000	6.7182	7.3126	5.3125	12.6264	0.3258	-0.034201 (4.1794, 0.2916)	0.509717 (8.5465, 0.7888)
1200	7.2940	8.8830	5.7589	14.6420	0.3536	-0.034204 (4.9622, 0.2847)	0.511906 (9.5968, 0.7746)
1400	7.8303	10.2386	6.2500	16.4886	0.3726	-0.034259 (5.6831, 0.2769)	0.513481 (10.6393, 0.7661)
1400 <sub>l</sub>	7.8284	10.2348	6.2530	16.4878	0.3726	-0.034259 (5.6831, 0.2769)	0.513481 (10.6392, 0.7661)
1500 <sub>l</sub>	8.2089	11.1191	6.5625	17.6816	0.3829	-0.035159 (6.8431, 0.2116)	0.514405 (11.4290, 0.7616)

## References

- Abdallah, S. (1987) "Numerical solutions for the pressure Poisson equation with Neumann boundary condition using a non-staggered grid. Part I", *J. Comput. Phys.* **70**, 182–192.
- Arakawa, A. (1966) "Computational design for long-term numerical integration of the equations of fluid motion: two-dimensional incompressible flow. Part I", *J. Comput. Phys.* **1**, 119–143.
- Armaly, B.F., Durst, F., Pereira, J.C.F. and Schonung, B. (1983) "Experimental and theoretical investigation of backward-facing step flow", *Fluid Mech.* **127**, 473–496.
- Barton, I.E. (1997) "The entrance effect of laminar flow over a backward-facing step geometry", *Int. J. Numer. Meth. Fluids* **25**, 633–644.
- Bruneau, C.-H. and Jouron, C. (1990) "An efficient scheme for solving steady incompressible Navier–Stokes equations", *J. Comput. Phys.* **89**, 389–413.
- Christov C.I. (1994) *Gaussian Elimination with Pivoting for Multi-diagonal Systems, Internal Report 4*. University of Reading.
- Christov, C.I. and Marinova, R.S. (1998a) "Implicit scheme for Navier–Stokes equations in primitive variables via vectorial operator splitting", *Notes on Numer. Fluid Mech.* **62**, 251–259, Wiesbaden, Vieweg.
- Christov, C.I. and Marinova, R.S. (1998b) "Numerical solutions for steady flow past a circular cylinder via method of variational imbedding", *Annuaire de l'Université de Sofia St. Kl. Ohridski* **90**, 177–189.
- Christov, C.I. and Marinova, R.S. (2001) "Implicit vectorial operator splitting for incompressible Navier–Stokes equations in primitive variables", *J. Comput. Technol.* **6**, 92–119.
- Douglas, J. and Rachford, H.H. (1956) "On the numerical solution of heat conduction problems in two and three space variables", *Trans. Amer. Math. Soc.* **82**, 421–439.
- Gartling, D. (1990) "A test problem for outflow boundary conditions-flow over a backward-facing step", *Int. J. Numer. Meth. Fluids* **11**, 53–967.
- Ghia, U., Ghia, K.N. and Shin, C.T. (1982) "High- $Re$  solutions for incompressible flow using the Navier–Stokes equations and a multigrid method", *J. Comput. Phys.* **48**, 387–411.
- Goodrich, J.W., Gustafson, K. and Halasi, K. (1990) "Hopf bifurcation in the driven cavity", *J. Comput. Phys.* **90**, 219–261.
- Goyon, O. (1996) "High-Reynolds number solutions of Navier–Stokes equation using incremental unknowns", *Comput. Meth. Appl. Mech. Eng.* **130**, 319–355.
- Gresho, P.M., Gartling, D.K., Torczynski, J.R., Cliffe, K.A., Winters, K.H., Garratt, T.G., Spence, A. and Goodrich, J.W. (1993) "Is a steady viscous incompressible two-dimensional flow over a backward-facing step at  $Re = 800$  stable?", *Int. J. Numer. Meth. Fluids* **17**, 501–541.
- Habashi, W.G., Peeters, M.F., Robichaud, M.P. and Nguyen, V-N. (1993) "A fully coupled finite element algorithm, using direct and iterative solvers, for the incompressible Navier–Stokes equations", *Incompressible Computational Fluid Dynamics: Trends and Advances* (Gunzburger and Nicolaides, Cambridge) pp 151–182.
- Hafez, M. and Soliman, M. (1993) "Numerical solution of the incompressible Navier–Stokes equations in primitive variables on unstaggered grids", *Incompressible Computational Fluid Dynamics: Trends and Advances* (Gunzburger and Nicolaides, Cambridge), pp 183–202.
- Kangro, U. and Nicolaides, R. (1999) "Divergence boundary conditions for vector Helmholtz equations with divergence constraints", *M<sup>2</sup>AN* **33**, 479–492.
- Keskar, J. and Lyn, D.A. (1999) "Computations of a laminar backward-facing step flow at  $Re = 800$  with a spectral domain decomposition method", *Int. J. Numer. Meth. Fluids* **29**, 411–427.
- Kim, J. and Moin, P. (1985) "Application of fractional-step method to incompressible Navier–Stokes equations", *J. Comput. Phys.* **59**, 308–323.
- Liao, S.J. and Zhu, J.M. (1996) "A short note on high-order stream function-vorticity formulation of 2D steady state Navier–Stokes equations", *Int. J. Numer. Meth. Fluids* **22**, 1–9.
- Mallison, G.D. and de Vahl Davis, G. (1973) "The method of false transients for the solution of coupled elliptic equations", *J. Comput. Phys.* **12**, 435–461.
- Marchuk, G.I. (1982) *Methods of Numerical Mathematics* (Springer, New York).
- Marinova, R.S., Christov, C.I. and Marinov, T.T. (2000) "High-Reynolds number solutions of incompressible Navier–Stokes equations using vectorial operator splitting", *Computational Fluid Dynamics* (Springer, Berlin) pp 247–252.
- Schreiber, R. and Keller, H.B. (1983) "Driven cavity flows by efficient numerical techniques", *J. Comput. Phys.* **49**, 310–333.
- Shankar, P.N. and Deshpande, M.D. (2000) "Fluid Dynamics in the Driven Cavity", *Annu. Ref. Fluid Mech.* **32**, 93–136.
- Shen, J. (1991) "Hopf bifurcation of the unsteady regularized driven cavity flow", *J. Comput. Phys.* **95**, 228–245.
- Soh, W.Y. (1987) "Time-marching solution of incompressible Navier–Stokes equations for internal flow", *J. Comput. Phys.* **70**, 232–252.
- Thompson, M.C. and Ferziger, J.H. (1989) "An adaptive multigrid technique for the incompressible Navier–Stokes equations", *J. Computat. Phys.* **82**, 94–121.
- Yanenko, N.N. (1971) *Method of Fractional Steps* (Springer, Berlin).